Prediction of Fiber Bragg Gratings Characteristics from Its Design Parameters Using Deep Learning

Ehsan Adibnia, Majid Ghadrdan[*], and Mohammad Ali Mansouri-Birjandi

Faculty of Electrical and Computer Engineering, University of Sistan and Baluchestan (USB), Zahedan, Iran

Corresponding author email: <u>Ghadrdan@ece.usb.ac.ir</u>

ABSTRACT— **This research addresses the complexities and inefficiencies encountered in fabricating fiber Bragg gratings (FBGs), which are crucial for applications in optical communications, lasers, and sensors. The core challenge lies in the intricate relationship between fabrication parameters and the FBG's physical properties, making optimization time-consuming. To circumvent these obstacles, the study introduces an artificial intelligence-based approach, utilizing a neural network to predict FBG physical parameters from transmission spectra, thereby streamlining the fabrication process. The neural network demonstrated exceptional predictive accuracy, significantly reducing the parameter prediction time from days to seconds. This advancement offers a promising avenue for enhancing the efficiency and precision of FBG sensor design and fabrication. The research not only showcases the potential of artificial intelligence in revolutionizing FBG production but also contributes to the broader field of optical technology by facilitating more rapid and informed design decisions, ultimately paving the way for developing more sophisticated and sensitive FBG-based applications.**

KEYWORDS: **Fiber Bragg Gratings, Optical Fiber, Deep Learning, Neural Network, Artificial Intelligence.**

I. INTRODUCTION

A fiber Bragg grating (FBG) is a short section of optical fiber, typically ranging from a few millimeters to a few centimeters, where the refractive index of the core region is periodically modulated on a sub-wavelength scale [1, 2]. FBGs have found wide applications in various fields, including optical communication systems as filters [3], lasers as cavity mirrors [4, 5], temperature [6], strain [7], and pressure [8] sensors with high sensitivity [9]. The typical transmission spectrum of an FBG is depicted in Fig.1. Three significant aspects are observed in the figure: firstly, the maximum reflectivity at the wavelength of 1550 nm; secondly, the Full-Width Half-Maximum (FWHM) where the FBG acts as a strong reflector; and thirdly, the series of distinct, narrow peaks known as Strength of sidelobe peaks. These elements are influenced by specific physical parameters of the FBG, such as its length, amplitude modulation index, apodization type, and period. The values of these parameters, in turn, depend on the fabrication process of the FBG, including factors such as laser pulse intensity, number of laser pulses, and fiber composition, referred to as fabrication parameters. In sensing applications, the objective is to generate slow-light peaks as narrow and strong as possible, necessitating the optimization of the fabrication parameters [2, 10]. However, this study faces several challenges. Firstly, the relationship between the fabrication and resulting physical parameters is poorly understood, often leading to a trial-and-error approach in determining the fabrication parameter values for FBG fabrication. Secondly, calculating the physical parameters from the measured transmission spectrum is non-trivial.
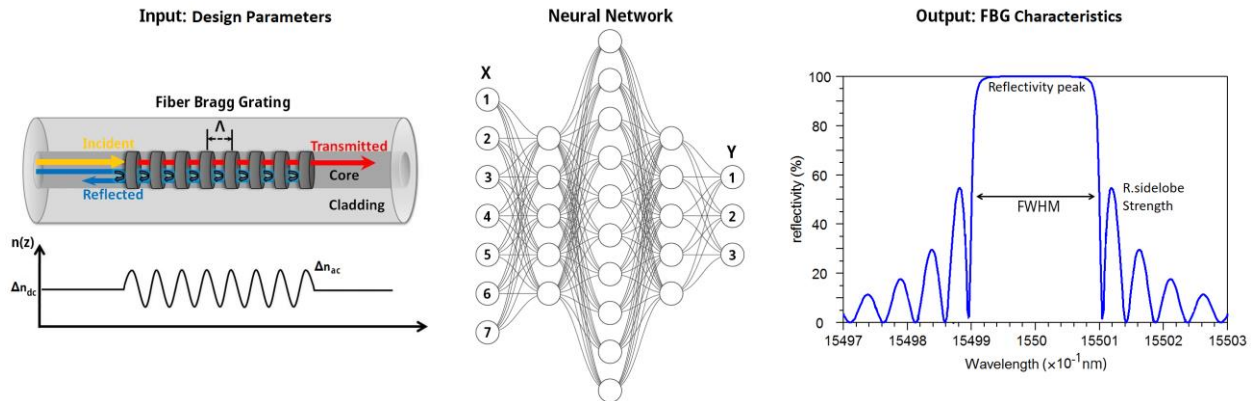
Fig. 1. The plan of the FBG structure and NN architecture for prediction of output parameters. An NN architecture was employed to predict the features of the FBG based on the design parameters.

A real-coded genetic algorithm was proposed for this calculation in [11, 12], while a Markov decision process was employed for optimizing similar structures [13]. Conversely, predicting the transmission spectrum from the physical parameter values is relatively straightforward using existing analytical methods, such as the Transfer Matrix Method (TMM) based on electromagnetic theory, which solves for the amplitudes of transmitted and reflected electric fields [14]. As a result, scientists, including many graduate students, frequently resort to the latter approach, spending days adjusting the physical parameter values until the calculated spectrum matches the measured spectrum. Unfortunately, the use of numerical solvers in simulations can be quite time-consuming and computationally expensive. This can be especially problematic in situations where real-time processing is necessary, such as with biosensors. The rapid progress of Artificial Intelligence (AI) has propelled Deep Learning (DL) to the forefront, recognizing it as an innovative technique to overcome current obstacles [15]. DL differs from traditional Machine Learning methods by exploiting the complex multilayer design of neural networks (NNs) to extract attributes at different scales and depths. This strategy notably enhances precision and efficiency in regression analyses. Consequently, there has been a surge in the implementation of DL across photonics fields [16].

This project introduces an NN that learns the correspondence between a transmission spectrum and its associated physical parameters to overcome the time-consuming fitting process. The network takes the features of the transmission spectrum as input and outputs a vector of predicted parameter values. This approach significantly reduces the time required to predict the physical parameters for a given spectrum, reducing it from days to seconds. This acceleration enhances research efforts to develop more advanced and highly sensitive FBG sensors.

II. THEORY AND MODELING

In this study, coupled mode theory is employed to analyze coupled-mode structures, while the TMM is utilized to solve the coupled mode equations. Light incident on an FBG is efficiently reflected when it satisfies the Bragg condition [17]:

$$\lambda_B = 2n_{eff} \Lambda, \tag{1}$$

where λ_B represents the Bragg wavelength, n_{eff} is the effective refractive index, and Λ denotes the grating period. The refractive index distribution $n(z)$ depicted in Fig. 1 can be expressed as follows [18]:

$$n(z) = n_0 + \Delta n_{dc}(z) + A(z)\Delta n_{ac}(z)\cos\left((2\pi/\Lambda)z + \theta(z)\right), \tag{2}$$

where n_0 represents the average refractive index change of the fiber core, $A(z)$ is the apodization function, Δn_{ac} represents the maximum index variation, Δn_{dc} is the average change in

refractive index, and θ denotes the period chirp. By applying the coupled mode theory, the reflectivity of a grating can be described as [18, 19]:

$$R\left(L,\lambda\right) = \frac{\kappa^2 \sinh^2\left(sL\right)}{\Delta\beta^2 \sinh^2\left(sL\right) + s^2 \cosh^2\left(sL\right)}, \quad (3)$$

where $R(L, \lambda)$ represents the reflectivity, L is the length of the grating, κ denotes the coupling constant, $\Delta\beta$ represents the detuning wave vector, and s is defined as $s=(\kappa^2-\Delta\beta^2)^{1/2}$. In a chirped FBG, the grating period varies along the length of the grating. The chirp coefficient influences the period as follows:

$$\text{period} - \left(\alpha/2\right) < \Lambda < \text{period} + \left(\alpha/2\right), \quad (4)$$

where α represents the chirp coefficient, and z varies between 0 and L. In this study, the following apodization functions are utilized for the design and simulation of an FBG [19]:

Uniform:

$$A\left(z\right) = 1 \quad -\frac{L}{2} \le z \le \frac{L}{2}, \quad (5)$$

Cosine:

$$A\left(z\right) = \cos\left(\frac{\pi z}{L}\right) \quad -\frac{L}{2} \le z \le \frac{L}{2}, \quad (6)$$

Raised-Cosine:

$$A\left(z\right) = \cos^2\left(\frac{\pi z}{L}\right) \quad -\frac{L}{2} \le z \le \frac{L}{2}, \quad (7)$$

Tanh:

$$A\left(z\right) = \frac{\tanh\left[\eta\left(1 - 2\left(\frac{z}{L}\right)\right)\right]}{\tanh\left(\eta\right)} \quad -\frac{L}{2} \le z \le \frac{L}{2}, \quad (8)$$

Here, the parameter η can be adjusted to modify the sharpness of the apodization profile. Figure 2 illustrates these apodization functions. In optical design, an apodization function is carefully designed and can be pretty intricate and tailored to meet specific system requirements and characteristics.
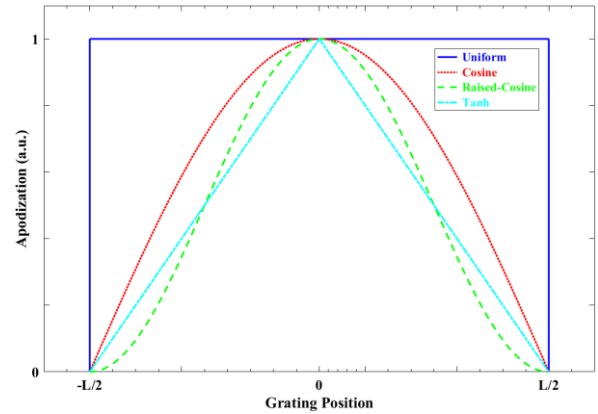

Fig. 2. The illustration of apodization functions. In optical design terminology, an apodization function refers to the intentional modification of an optical system's input intensity profile. This function may be complex and carefully created to customize the system to specific characteristics.

III. METHOD OF DL IMPLEMENTATION

The primary objective of this research is to utilize a vector containing the normalized physical parameters of an FBG as input to generate a corresponding measured transmission spectrum (refer to Fig. 1). Several encoding methods can be considered for the input data:

1. Image representation: Using an image of the transmission spectrum, although feasible, presents challenges. To accurately capture the number, height, and width of the numerous slow-light peaks on the left edge of the spectrum, high-resolution images of at least 1080×1080 or larger would be required. However, processing such images can significantly slow down data processing, and encoding the image can result in information loss. Therefore, this method is not the most accurate for representing the data.

2. Vectorization of the spectrum: Another approach is to vectorize the transmission spectrum as (x1(i), x2(i)), where x1(i) represents a vector of wavelengths ranging from 1550 nm to 1560 nm, and x2(i) represents a vector of the corresponding transmitted power T at those wavelengths. However, this method leads to significant

and cumbersome weight matrices, challenging training and storage.

3. Parameterization of the input data: The preferred approach is to parameterize the input data.

It is important to note that the spectra are highly dependent on the parameter values and must be carefully encoded to enable accurate predictions by the NN. The provided formulas establish the relationship between these inputs and the desired outputs. In the next section, we will present the correlation of these parameters in more detail, including simulation justifications. Furthermore, since there is no publicly available dataset for this problem, we generated our dataset in-house. We trained the NN using standardized FBG design parameters, resulting in a normalized spectrum consisting of 30 data points. The thorough investigation carried out in this work generated a comprehensive training dataset consisting of 1.5×10^4 unique samples, each of which was carefully produced through rigorous Finite-Difference Time-Domain (FDTD) simulations. The total number of samples was divided into training, validation, and test datasets, with a ratio of 70% for training, 15% for validation, and 15% for testing. The training process employed a batch size of 40 and continued until improvements in the validation loss stopped, with updates based on gradients computed from the training loss. The data figures shown in this paper were drawn exclusively from the validation set and were not used during the actual training phase. The model's capacity to generalize to new, unseen data depended critically on the appropriate selection of hyperparameters, such as batch size, number of training iterations, and the learning rate. Throughout the 250 training epochs, a constant learning rate of 0.05 was maintained.

The NN architecture employed in this study consisted of three fully connected dense layers. This NN identifies complex relationships between input parameters and the resulting transmission spectrum, giving a more comprehensive understanding of the FBG's behavior and performance. The hidden units of

these layers were set to 25, 50, and 25, respectively, as illustrated in Fig. 1 (In this figure, each node represents five neurons). ReLU activation was utilized in the initial layers, while the last layer employed a sigmoid activation function to ensure output values were constrained within the range of 0 and 1.

The mean squared error (MSE) was selected as the loss metric for evaluating the network's performance and optimizing the weights. The MSE measures the average squared difference between the predicted and actual values, as depicted by the specified MSE function.

$$\text{MSE} = \frac{1}{n} \sum_{i=1}^{n} \left(y_{pred} - y_{true} \right)^2, \tag{9}$$

where n denotes the total number of data points, y_{pred} is the predicted value, and y_{true} represents the actual value computed utilizing the FDTD method.

The Adam optimizer was employed in this study, utilizing the default parameters introduced in the original publication [20]. The NN implementation was facilitated using the Keras library [21], a Python-based DL library that operates on top of TensorFlow [22], an open-source Python library. Keras and Tensorflow were chosen due to their convenient helper functions, which greatly simplified and expedited the development of this DL approach.

IV. RESULTS AND DISCUSSION

The parameters used for simulation are shown in Table 1. Based on the described model and some significant practical considerations that should be considered when designing an FBG, we investigate the effects of input parameters on the outputs in the following subsections.

Table 1. The parameters used in the simulation.

Parameter	Quantity
Free space wavelength, (nm)	1550
Period, (μm)	0.5
Modulation depth	0.0003
Cladding index	1.45
Waveguide width and height (μm)	5.25

A. *Index Difference*

An increase in index difference causes an increase in reflectivity, bandwidth, and sidelobe strength, so this increase is not the same at different lengths. The reflectivity, bandwidth, and sidelobe strength variation are calculated when the index difference varies from 0.01 to 0.1 and 0.1 to 0.2. This result demonstrates that the increase of undesirable characteristics, such as sidelobe strength, is greater than desirable characteristics, such as reflectivity, when the index difference varies from 0.1 to 0.2. Therefore, index differences greater than 0.1 are not suitable. The increase in sidelobe strength is remarkable and, therefore, must be reduced. In the next section, we will examine methods of reducing sidelobe strength.

B. *Apodization*

Apodization is a technique that reduces the sidelobe strength. The functions that have been used in apodization are as follows: Cosine, Raised-Cosine, and Tanh. These functions will be applied to the FBG and evaluated in this section. Figure 3a illustrates how the apodization process decreases the reflectivity. It is observed that the reflectivity increases with an increase in grating length and reaches 100% at the approximate length of 15mm for the case of uniform FBG, 25mm for Cosine apodized FBG, and 30mm for both Raised-Cosine and Tanh apodized FBG. Figure 3a also shows that the Raised-Cosine and Tanh-applied FBG reflectivities are the same, and the Cosine profile has the highest reflectivity.

Sidelobe strength reduction is the main effect of applying apodization. This reduction depends on apodization profiles and is different at various lengths. The relationship between apodized FBG Sidelobe strength and grating length has been illustrated in Fig. 3b. Nonlinear changes in the Sidelobe strength with increasing grating length can be observed in Fig. 3b. As can be seen in this figure, the Raised-Cosine profile has the lowest Sidelobe strength. The selection of an appropriate bandwidth depends on the applications. The wider bandwidth is a key parameter for uncooled pump laser applications. Also, the

FBGs with wider bandwidths are required in the FBG stabilizer design [23] and ultrasonic detectors [24].
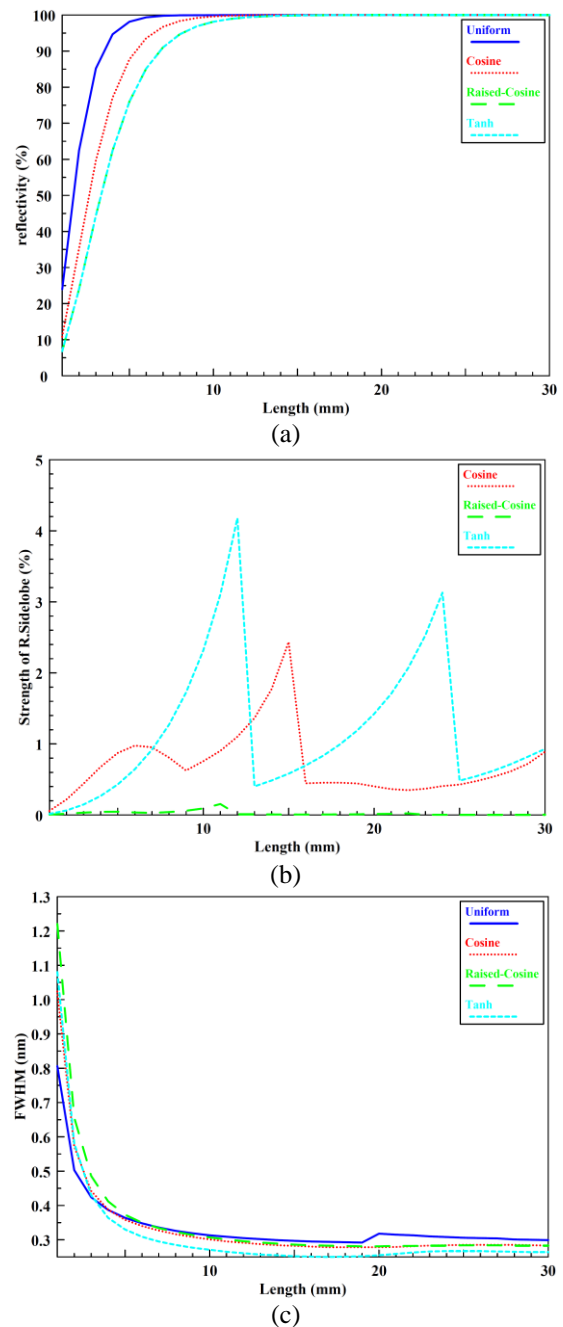

(a)

(b)

(c)

Fig. 3. (a) shows that the reflectivity of apodized FBGs increases with grating length. The cosine profile has the highest reflectivity. (b) shows that the Raised-Cosine profile has the lowest sidelobe strength. (c) shows that the Raised-Cosine profile has the highest bandwidth.

In the sensing applications, The FBGs have better resolution with narrower bandwidth and can achieve higher measurement speed [18]. However, the optical signal-to-noise ratio of the long-distance point sensing system decreases

169

gradually when the bandwidth of the FBG increases. Fig. 3c demonstrates that applying apodization can change the bandwidth. As is observed from Fig. 3©, the Raised-Cosine profile provides the highest bandwidth among the simulated apodized profiles.

C. *Deep Learning Technique*

As anticipated, the training loss decreased as the number of epochs increased, as illustrated in Fig. 4. The training loss rapidly converged to a low value of 0.055 after 250 epochs. Notably, the error on the validation set closely aligned with the training set, which was expected since they originated from the same distribution. This indicates that the network did not overfit the training data. Expanding the width or size of the network did not yield significant improvements in performance.
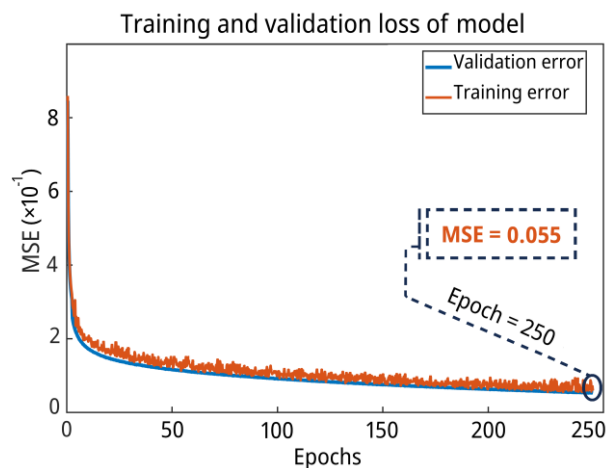

Fig. 4. The graph displays the NN's ability to estimate the spectrum. It shows the training loss, which indicates significant decreases. This drop suggests that the NN can recognize patterns in the data.

This observation suggests that enhancements may be required in the training dataset size and/or the encoding of input features. Given the relatively small dataset, iterating through the entire dataset per epoch did not impose a significant time burden. Thus, the batch size was maintained equal to the number of training samples. However, it may be necessary to reduce the batch size in future endeavors involving larger datasets. Table 2 presents two examples from the test set, demonstrating instances where the ground truth and predicted parameter values exhibit an excellent match.

The term "ground truth" refers to the known or accepted data used as a benchmark or reference point for training and evaluating machine learning models.

Table **2**. DL's predicted characteristics of FBG compared to its actual characteristics.

FBG	Reflectivity (%)		Sidelobe strength (%)		Bandwidth (nm)	
	FDTD	DL	FDTD	DL	FDTD	DL
Uniform	100	100	75.10	75.15	0.30	0.29
Cosine	100	100	0.40	0.42	0.30	0.29
Raised-Cosine	100	100	0.00	0.00	0.30	0.27
Tanh	100	100	0.91	0.90	0.25	0.28

It represents the true or definitive information about a dataset, essential for supervised learning tasks where the model aims to predict or classify the target variable accurately. The strong correspondence between the values further confirms the approach's effectiveness in learning the relationship between the input and output. We recognize that dedicating additional efforts to refining this approach can yield even more remarkable results. Nonetheless, the primary objective of this research is to showcase the potential of AI in predicting desired parameters for FBG designers. Using approaches that automatically identify spectral features, such as long short-term memory (LSTM), as opposed to manually engineering features as done in this study, may potentially enhance performance in such cases. These aspects can be further investigated and explored in future research endeavors, providing opportunities to expand upon the findings and delve deeper into the subject matter.

D. *Study Limitations*

As we approach the conclusion of this work, it is only fair that we critically scrutinize these achievements. Although the NN developed in this study effectively predicts the transmission spectra for various types of FBGs, such as uniform, apodized, and linearly chirped designs, it currently does not extend to specific specialized FBG structures. Specifically, the model lacks training for highly complex configurations like tilted FBGs or nonlinearly chirped FBGs, which require advanced

fabrication techniques. This limitation arises from two main factors: First, these specialized FBG types represent only a tiny portion of FBG devices used in practical applications. Second, accurate modeling these complex structures would necessitate a considerable increase in the number of input parameters for the NN, thereby requiring a significantly larger training dataset that is not currently available. Nonetheless, we acknowledge the need to enhance the proposed model's generalization capabilities continually. With access to more computational resources and a more extensive FBG structural dataset, future research could aim to incorporate the parameters needed to predict the transmission spectra of tilted and nonlinearly chirped FBGs. This would enable the NN to offer a comprehensive solution for modeling FBG devices, thereby broadening its practical applicability to a broader array of photonic technologies.

V. CONCLUSION

This study has leveraged the power of deep learning (DL) to establish a strong correlation between the transmission spectrum characteristics of fiber Bragg gratings (FBGs) and their operational effectiveness. Our research has demonstrated the ability of DL techniques to navigate the complexities of inverse design, significantly enhancing the capabilities of FBGs. The neural network (NN) models developed as part of this work have rapidly converged and provided detailed predictions of the spectral features for various FBG spatial configurations.

Notably, the NN models have shown the remarkable ability to closely align the predicted transmission spectra with those obtained from rigorous finite-difference time-domain (FDTD) simulations, highlighting the exceptional precision of our deep learning approach. This method has substantially reduced the computational demands compared to traditional numerical solvers, enabling swift and cost-effective spectral predictions for FBGs. Furthermore, our methodology has successfully overcome the longstanding challenge of inverse design, empowering the creation of optimal

FBG geometries that produce the desired optical response spectra.

The validation of our DL model has been based on spectra from physically realizable FBG configurations, underscoring the potential for integrating NN-enabled FBGs into optical communications systems. This validation emphasizes the practical significance of our findings, demonstrating their applicability across real-world contexts, including all-optical signal processing and communication.

The combination of the precision of nanotechnology and the computational power and pattern recognition capabilities of artificial intelligence is ushering in a new era of scientific innovation. This convergence promises to unleash groundbreaking discoveries and drive innovative applications, marking a transformative shift in scientific exploration with the potential to revolutionize numerous fields, including the design and fabrication of FBG-based sensors and devices.

REFERENCES

[1] L.A. Ngiejungbwen, H. Hamdaoui, and M.-Y. Chen, "Polymer optical fiber and fiber Bragg grating sensors for biomedical engineering Applications: A comprehensive review," Opt. Laser Technol., Vol. 170, pp., 110187(1-40), 2024.

[2] H. Saghaei, P. Elyasi, and B.J. Shastri, "Sinusoidal and rectangular Bragg grating filters: Design, fabrication, and comparative analysis," J. Appl. Phys., Vol. 132, pp., 064501(1-11), 2022.

[3] Q. Zhang, X. Han, X. Fang, M. Liu, K. Ge, H. Jiang, W. Dong, and X. Zhang, "A single passband microwave photonic filter with enhanced flat top and shape factor based on tunable optical bandpass filter and fiber Bragg gratings," Opt. Laser Technol., Vol. 168, pp. 109838(1-30), 2024.

[4] Z. Zhang, F. Liu, X. Guo, T. Chen, L. Han, and W. Zhang, "Optimization of Dual-Wavelength linear cavity Erbium-Doped fiber laser based on pairs of fiber Bragg gratings," Opt. Fiber Technol., Vol. 83, pp. 103675(1-6), 2024.

[5] B. Jafari and E. Gholizadeh, "Multifunctional graphene-based optoelectronic structure based

on a Fabry–Perot cavity enhanced by a metallic nanoantenna," Appl. Opt., Vol. 61, pp. 10658-10668, 2022.

[6] C. Li, X. Tong, W. Huang, Y. Wang, F. Zeng, L. Chen, X. Shi, and C. Zeng, "Development of a Fast Response, High Accuracy, and Miniaturized Fiber Bragg Grating (FBG) sensor for Fluid Temperature measurement," IEEE Sens. J., Vol. 24, pp. 8746-8753, 2024.

[7] J. He, Z. Li, X. Xu, Q. Tan, X. Weng, L. Liu, J. Qu, C. Liao, and Y. Wang, "High-temperature strain sensor based on sapphire fiber Bragg grating," Opt. Lett., Vol. 49, pp. 446-449, 2024.

[8] B. Xu, G. Chen, X. Xu, S. Liu, C. Liao, X. Weng, L. Liu, J. Qu, Y. Wang, and J. He, "Highly birefringent side-hole fiber Bragg grating for high-temperature pressure sensing," Opt. Lett., Vol. 49, pp. 1233-1236, 2024.

[9] B. Jafari, E. Gholizadeh, B. Jafari, M. Zhoulideh, E. Adibnia, M. Ghafariasl, M. Noori, and S. Golmohammadi, "Highly sensitive label-free biosensor: graphene/CaF2 multilayer for gas, cancer, virus, and diabetes detection with enhanced quality factor and figure of merit," Sci. Rep., Vol. 13, pp. 16184(1-15), 2023.

[10] Q. Chen, J.-S. Boisvert, M.S. Sharawi, and R. Kashyap, "Bragg gratings with novel waveguide models fabricated in bulk glass via fs-laser writing and their slow-light effects," Opt. Express, Vol. 32, pp. 188-204, 2024.

[11] A. Rostami and A. Yazdanpanah-Goharriz, "A new method for classification and identification of complex fiber Bragg grating using the genetic algorithm," Prog. Electromagn. Res., Vol. 75, pp. 329-356, 2007.

[12] G. Cormier, R. Boudreau, and S. Thériault, "Real-coded genetic algorithm for Bragg grating parameter synthesis," J. Opt. Soc. Am. B, Vol. 18, pp. 1771-1776, 2001.

[13] W. Ye, B. Gu, and Y. Wang, "Airborne distributed position and orientation system transfer alignment method based on fiber bragg grating," Sensors, Vol. 20, pp. 2120(1-19), 2020.

[14] T. Agliullin, V. Anfinogentov, O. Morozov, A. Sakhabutdinov, B. Valeev, A. Niyazgulyeva, and Y. Garovov, "Comparative analysis of the methods for fiber Bragg structures spectrum modeling," Algorithms, Vol. 16, pp. 101(1-15), 2023.

[15] M. Farrokhi, F. Taheri, E. Adibnia, S. Mehrtabar, Z. Rassaf, S.H. Tooyserkani, Y. Rajabloo, G.S. Tooyserkani, Z. Ranjbar, and E. Hashemi, *The AI Diagnostician: Improving Medical Diagnosis with Artificial Intelligence* Kindle. pp. 1-219, 2024.

[16] E. Adibnia, M.A. Mansouri-Birjandi, M. Ghadrdan, and P. Jafari, "A deep learning method for empirical spectral prediction and inverse design of all-optical nonlinear plasmonic ring resonator switches," Sci. Rep., Vol. 14, pp. 5787(1-17), 2024.

[17] K. Abdelsalam, E. Ordouie, M.G. Vazimali, F.A. Juneghani, P. Kumar, G.S. Kanter, and S. Fathpour, "Tunable dual-channel ultra-narrowband Bragg grating filter on thin-film lithium niobate," Opt. Lett., Vol. 46, pp. 2730-2733, 2021.

[18] N.A. Mohammed, T.A. Ali, M.H. Aly, and O. Member, "Evaluation and performance enhancement for accurate FBG temperature sensor measurement with different apodization profiles in single and quasi-distributed DWDM systems," Opt. Lasers Eng., Vol. 55, pp. 22-34, 2014.

[19] H. Zhang, "A novel method of optimal apodization selection for chirped fiber Bragg gratings," Optik, Vol. 125, pp. 1646-1649, 2014.

[20] D.P. Kingma and J. Ba, "Adam: A method for stochastic optimization," arXiv preprint arXiv:1412.6980, 2014.

[21] N. Ketkar, *Introduction to keras*, in *Deep learning with python: a hands-on introduction*, pp. 97-111, 2017.

[22] M. Abadi, P. Barham, J. Chen, Z. Chen, A. Davis, J. Dean, M. Devin, S. Ghemawat, G. Irving, and M. Isard, "{TensorFlow}: a system for {Large-Scale} machine learning," in 12th USENIX symposium on operating systems design and implementation (OSDI 16), pp. 265-283, 2016.

[23] Y. Zhao, R. Hou, and C. Zhou, "Writing wide bandwidth nonchirped fiber Bragg gratings with high sidelobe suppression ratio by linearly scaling apodization," Opt. Eng., Vol. 49, pp. 085001(1-5), 2010.

[24] C. Li, X. Peng, J. Liu, C. Wang, S. Fan, and S. Cao, "D-shaped fiber Bragg grating ultrasonic hydrophone with enhanced sensitivity and

bandwidth," J. Lightwave Technol., Vol. 37, pp. 2100-2108, 2019.

Ehsan Adibnia was born in Zabol in 1988. He received his B.Sc. and M.Sc. in electrical engineering from the University of Sistan and Baluchestan, Iran, in 2011 and 2014, respectively. He is currently a Ph.D. candidate at this university.

He has gained extensive work experience in nanophotonics. Currently, he holds the position of Electrical Laboratory Supervisor at the University of Sistan and Baluchestan. He has made significant contributions to nanophotonics, focusing on artificial intelligence. His main research interests include photonics, optics, plasmonics, graphene, and multidisciplinary science.

As a respected professional in photonics, Mr. Adibnia is actively involved in the Optics and Photonics Society of Iran and has reviewed various articles.

Majid Ghadrdan was born in Zabol in 1988. He received his Ph.D. in electrical engineering from the University of Sistan and Baluchestan, Iran in 2018. After completing his doctoral studies, he joined the University of Sistan and Baluchestan as an assistant professor, where he continues to contribute to the academic community.

He has made significant contributions to the field, with a focus on nonlinear optics, plasmonics, and photonic crystals. As a respected professional in optics, Dr. Ghadrdan is actively involved in several professional societies, including the Optics and Photonics Society of Iran and the Iranian Society of Engineering Education. He has served as an editor for the International Journal of Industrial Electronics, Control, and Optimization (IECO), as well as a reviewer for numerous esteemed journals and conferences.

Mohammad Ali Mansouri-Birjandi was born in Birjand in 1961. He received his Ph.D. in electronic engineering from Tarbiat Modares University, Tehran, Iran in 2009. His major field of study is photonics.

He has gained extensive work experience in photonic engineering. Currently, he holds the position of professor at the University of Sistan and Baluchestan. He has made significant contributions to the field, with a focus on plasmonics. Dr Mansouri is also interested in photonics engineering and nanophotonics.

As a respected professional in photonics, Prof. Mansouri-Birjandi is actively involved in several professional societies, including the Optics and Photonics Society of Iran, the Iranian Society of Engineering Education, and the Iranian Association of Electrical and Electronic Engineers (IAEEE). He has been recognized for his accomplishments and has received the top 2% most cited scientist in the world in 2022 to 2024.

THIS PAGE IS INTENTIONALLY LEFT BLANK.